Electronic Supporting Information

Near thermal, selective liberation of hydrogen from formic acid catalysed by copper hydride ate complexes

Howard Z. Ma,[a] Allan J. Canty,[b] and Richard A. J. O'Hair*[a]

(a) School of Chemistry and Bio21 Molecular Science and Biotechnology Institute, University of Melbourne, 30 Flemington Rd, Parkville, Victoria 3010, Australia. Fax: (+) 61 3 9347 8124; E-mail: rohair@unimelb.edu.au

(b) School of Natural Sciences – Chemistry, University of Tasmania, Private Bag 75, Hobart, Tasmania, 7001, Australia.

Contents of Supplementary Information

S1. Gas-phase characterisation of copper hydrides

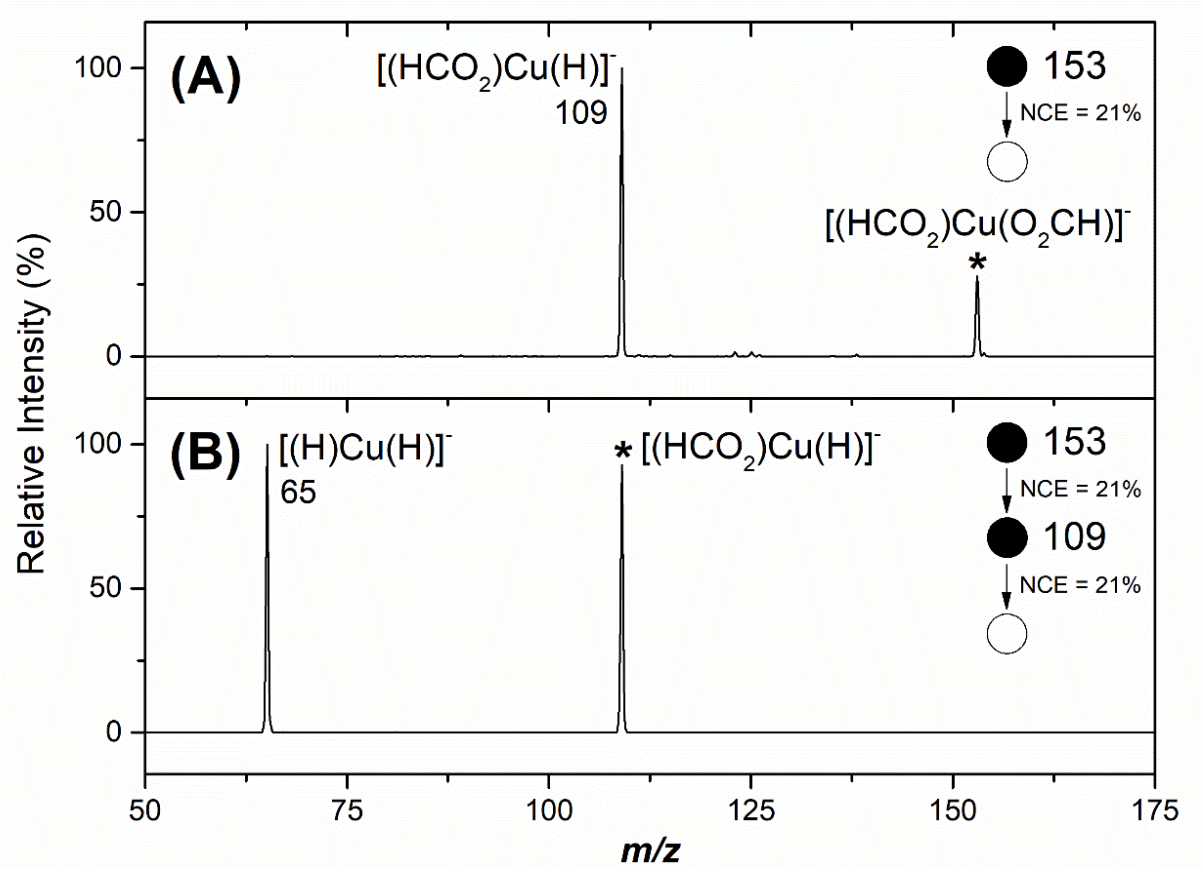

Figure S1. LTQ ESI-MS^n CID spectra showing decarboxylation from the precursor ion $[Cu(O_2CH)_2]^-$ (*m/z* 153) formed from an acetonitrile mixture of copper(I) oxide and formic acid, obtained using a typical Q value of 0.25, an activation time of 10 ms with the stated Normalized Collision Energies (NCE): (A) CID-MS^2 spectrum of decarboxylation from $[(HCO_2)Cu(O_2CH)]^-$ (*m/z* 153) to give $[(HCO_2)Cu(H)]^-$ (*m/z* 109) (NCE = 21%); (B) CID-MS^3 spectrum of decarboxylation from $[(HCO_2)Cu(H)]^-$ (*m/z* 109) to give $[(H)Cu(H)]^-$ (*m/z* 65) (NCE = 21%). An asterisk (*) denotes the mass selected precursor ion.

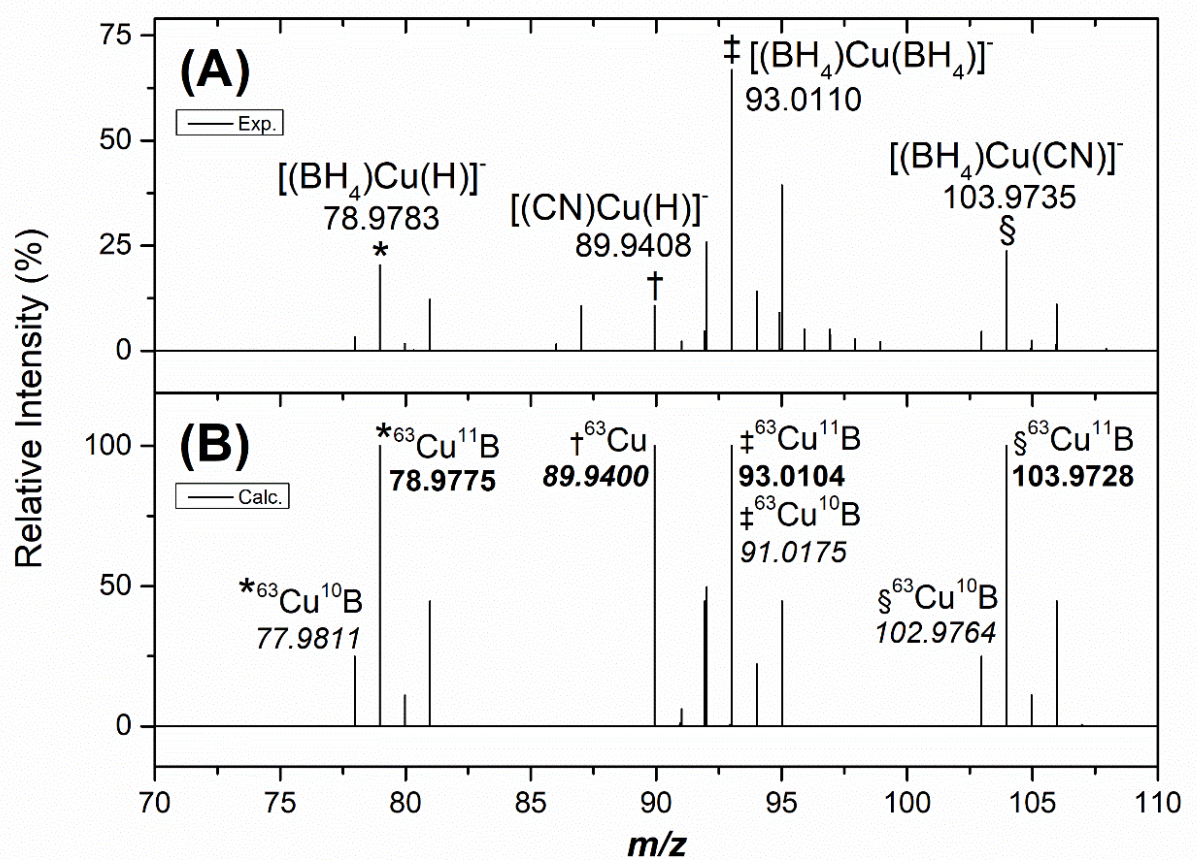

Figure S2. Orbitrap negative ion mode ESI-MS mass spectrum of an acetonitrile solution of copper(I) phenylacetylide with a 10-fold excess of sodium borohydride ($NaBH_4$) showing the formation of mononuclear cuprates: (A) *: $[(BH_4)Cu(H)]^-$ (*m/z* 78.9783), †: $[(CN)Cu(H)]^-$ (*m/z* 89.9408), ‡: $[(BH_4)Cu(BH_4)]^-$ (*m/z* 93.0110) and §: $[(BH_4)Cu(CN)]^-$ (*m/z* 103.9735). *m/z* values shown are of the most intense peak in the isotopic envelope of the complex; (B) Theoretical isotope patterns of the mentioned cuprates and their accurate masses (the monoisotopic mass is denoted in italics and the most abundant mass is denoted in bold).

S2. High resolution mass spectrometry (HRMS) data

Table S1. HRMS experiments (Orbitrap Elite ETD linear ion trap mass spectrometer) confirming assignments of key mononuclear cuprate complexes.

Ion	**Molecular Formula**	**Exact mass – calculated (*m/z*)**	**Exact mass – experimental (*m/z*)**	**Mass error (ppm)**
$[(BH_4)Cu(H)]^-$	Cu1 H5 B1	78.9775	78.9783	10.1
$[(CN)Cu(H)]^-$	Cu1 N1 C1 H1	89.9400	89.9408	7.8
$[(BH_4)Cu(BH_4)]^-$	Cu1 H8 B2	93.0104	93.0110	6.5

$[(BH_4)Cu(CN)]^-$	Cu1 H5 B1 N1 C1	103.9728	103.9735.	5.8

Table S2. HRMS experiments (Orbitrap Elite ETD linear ion trap mass spectrometer) confirming assignments of key product ions formed in the ion-molecule reactions between $[(L)Cu(H)]^-$, where L = H^-, HCO_2^-, BH_4^- and CN^-, with formic acid (HCO_2H) and d_1-formic acid (DCO_2H).

Ion	**Molecular Formula**	**Exact mass – calculated (*m/z*)**	**Exact mass – experimental (*m/z*)**	**Mass error (ppm)**
$[(H)Cu(H)]^-$	Cu1 H2	64.9447	64.9457	15.4
$[(H)Cu(D)]^-$	Cu1 H1 D1	65.9510	65.9520	15.2
$[(D)Cu(D)]^-$	Cu1 D2	66.9573	66.9583	14.9
$[(H)Cu(O_2CH)]^-$	Cu1 H1 O2 C1	108.9345	108.9353	7.3
$[(H)Cu(O_2CD)]^-$	Cu1 H1 D1 C1 O2	109.9408	109.9416	7.3
$[(D)Cu(O_2CD)]^-$	Cu1 D2 C1 O2	110.9471	110.9478	6.3
$[(DCO_2)Cu(O_2CD)]^-$	Cu1 D2 C2O4	154.9369	154.9377	5.2
$[(HCO_2)Cu(O_2CH)]^-$	Cu1 H2 O4 C2	152.9244	152.9252	5.2
$[(BH_4)Cu(H)]^-$	Cu1 H5 B1	78.9775	78.9783	10.1
$[(BH_4)Cu(D)]^-$	Cu1 H4 D1 B1	79.9838	79.9846	10.0
$[(BH_4)Cu(O_2CH)]^-$	Cu1 B1 H5 O2 C1	122.9673	122.9680	5.7
$[(BH_4)Cu(O_2CD)]^-$	Cu1 B1 H4 D1 O2 C1	123.9736	123.9743	5.6
$[(CN)Cu(H)]^-$	Cu1 N1 C1 H1	89.9400	89.9408	8.9
$[(CN)Cu(D)]^-$	Cu1 N1 C1 D1	90.9462	90.9470	8.8

$[(CN)Cu(O_2CD)]^-$	Cu1 C2 N1 O2 D1	134.9361	134.9369	5.9

S3. MS^n spectra for the IMR with HCO_2H

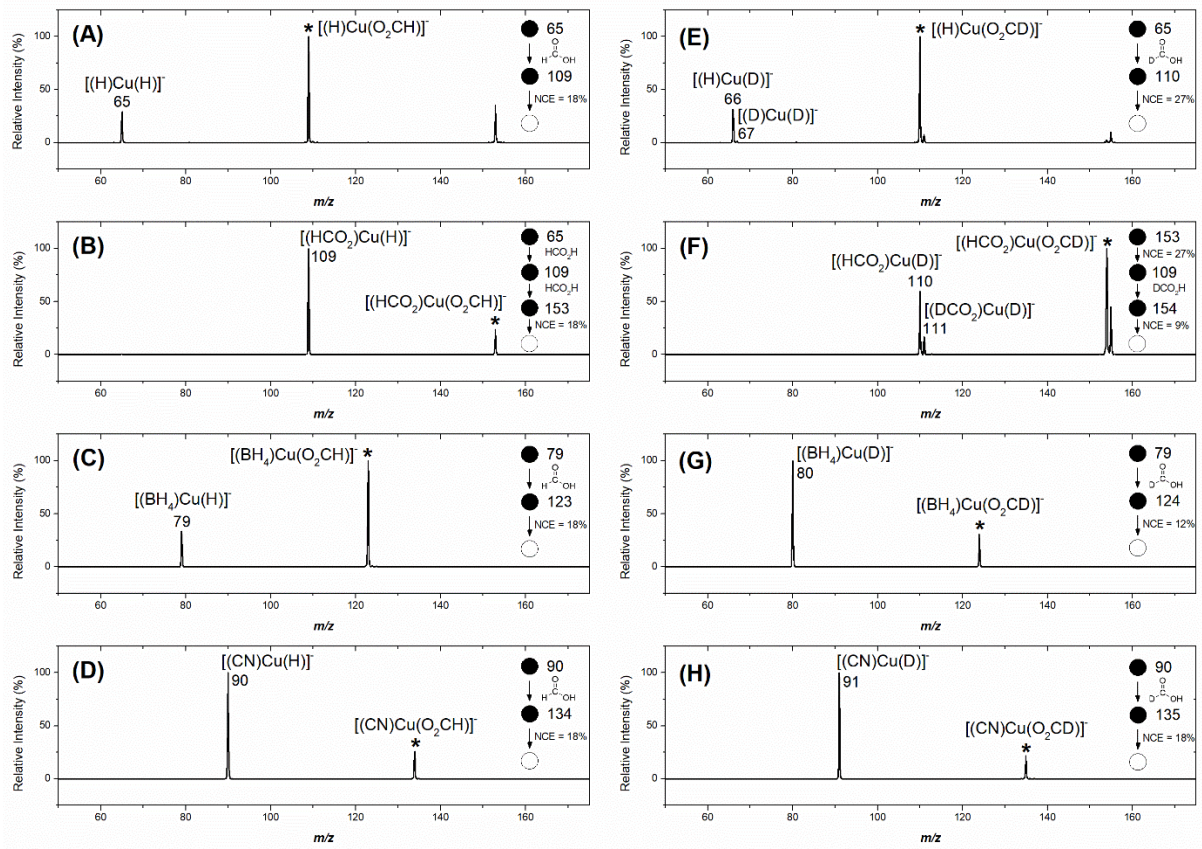

Figure S3. Low energy ion trap collision-induced dissociation (CID) experiments on coordinated formate copper 'ate' complexes $[(L)Cu(O_2CH)]^-$ or $[(L)Cu(O_2CD)]^-$, where L = H^-, O_2CH^-, BH_4^-, CN^-, obtained using a typical Q value of 0.25, an activation time of 10 ms with the stated Normalized Collision Energies (NCE). (A) MS^3 on $[(H)Cu(O_2CH)]^-$ (*m/z* 109) (NCE = 18%); (B) MS^4 on $[(HCO_2)Cu(O_2CH)]^-$ (*m/z* 153) (NCE = 18%); (C) MS^3 on $[(BH_4)Cu(O_2CH)]^-$ (*m/z* 123) (NCE = 18%); (D) MS^3 on $[(CN)Cu(O_2CH)]^-$ (*m/z* 134) (NCE = 18%); (E) MS^3 on $[(H)Cu(O_2CD)]^-$ (*m/z* 110) (NCE = 27%); (F) MS^4 on $[(HCO_2)Cu(O_2CD)]^-$ (*m/z* 154) (NCE = 9%); (G) MS^3 on $[(BH_4)Cu(O_2CD)]^-$ (*m/z* 124) (NCE = 12%), and; (H) MS^3 on $[(CN)Cu(O_2CD)]^-$ (*m/z* 135) (NCE = 18%). An asterisk (*) denotes the mass selected precursor ion.

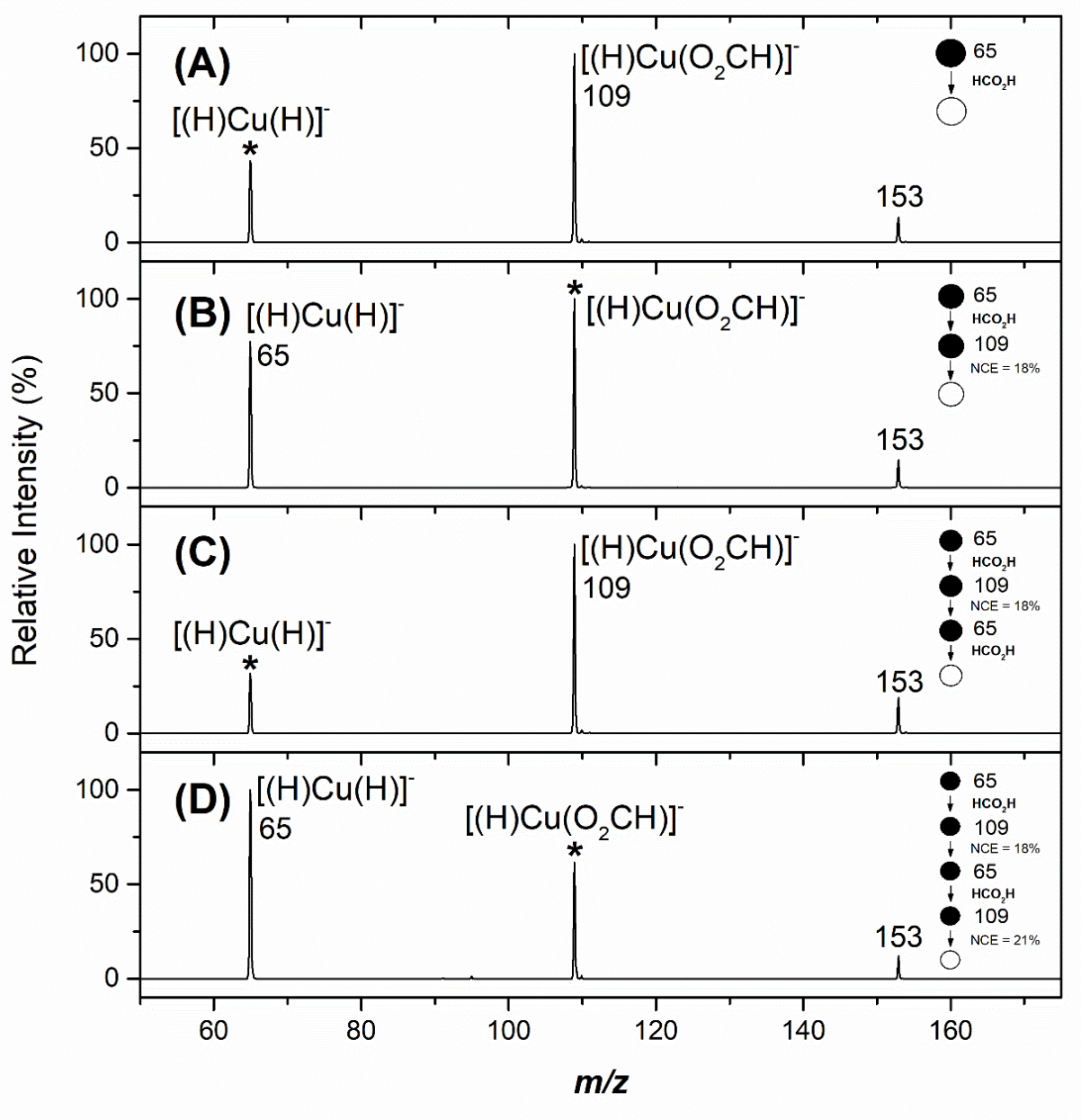

Figure S4. Multistage mass spectrometry (MS^n) on $[(L)Cu(H)]^-$, L = H^-, demonstrating its involvement in a two-step gas-phase catalytic cycle for the selective decomposition of formic acid: (A) MS^2 IMR experiment of $[(H)Cu(H)]^-$ (*m/z* 65), **1_H**, with HCO_2H; (B) MS^3 low energy ion trap collision-induced dissociation (CID) experiment on $[(H)Cu(O_2CH)]^-$ (*m/z* 109); (C) MS^4 IMR experiment of $[(H)Cu(H)]^-$ (*m/z* 65), **1_H**, with HCO_2H, and; (D) MS^5 low energy ion trap collision-induced dissociation (CID) experiment on $[(H)Cu(O_2CH)]^-$ (*m/z* 109). An asterisk (*) denotes the mass selected precursor ion. The peak at 153 *m/z* is the product ion $[(HCO_2)Cu(O_2CH)]^-$.

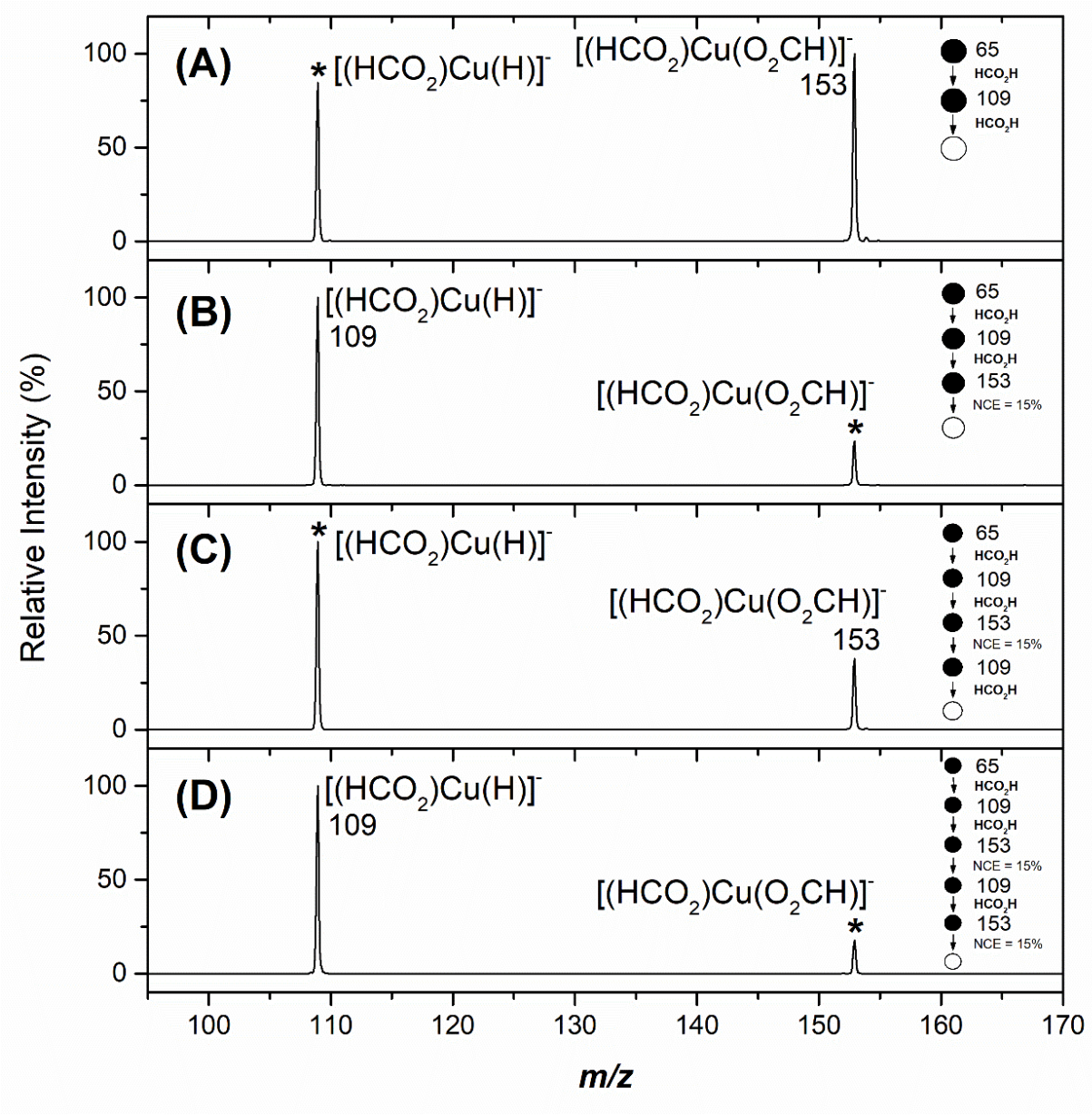

Figure S5. Multistage mass spectrometry (MS^n) on $[(L)Cu(H)]^-$, L = O_2CH^-, demonstrating its involvement in a two-step gas-phase catalytic cycle for the selective decomposition of formic acid: (A) MS^3 IMR experiment of $[(HCO_2)Cu(H)]^-$ (*m/z* 109), **1_O₂CH**, with HCO_2H; (B) MS^4 low energy ion trap collision-induced dissociation (CID) experiment on $[(HCO_2)Cu(O_2CH)]^-$ (*m/z* 153); (C) MS^5 IMR experiment of $[(HCO_2)Cu(H)]^-$ (*m/z* 109), **1_O₂CH**, with HCO_2H, and; (D) MS^6 low energy ion trap collision-induced dissociation (CID) experiment on $[(HCO_2)Cu(O_2CH)]^-$ (*m/z* 153). An asterisk (*) denotes the mass selected precursor ion.

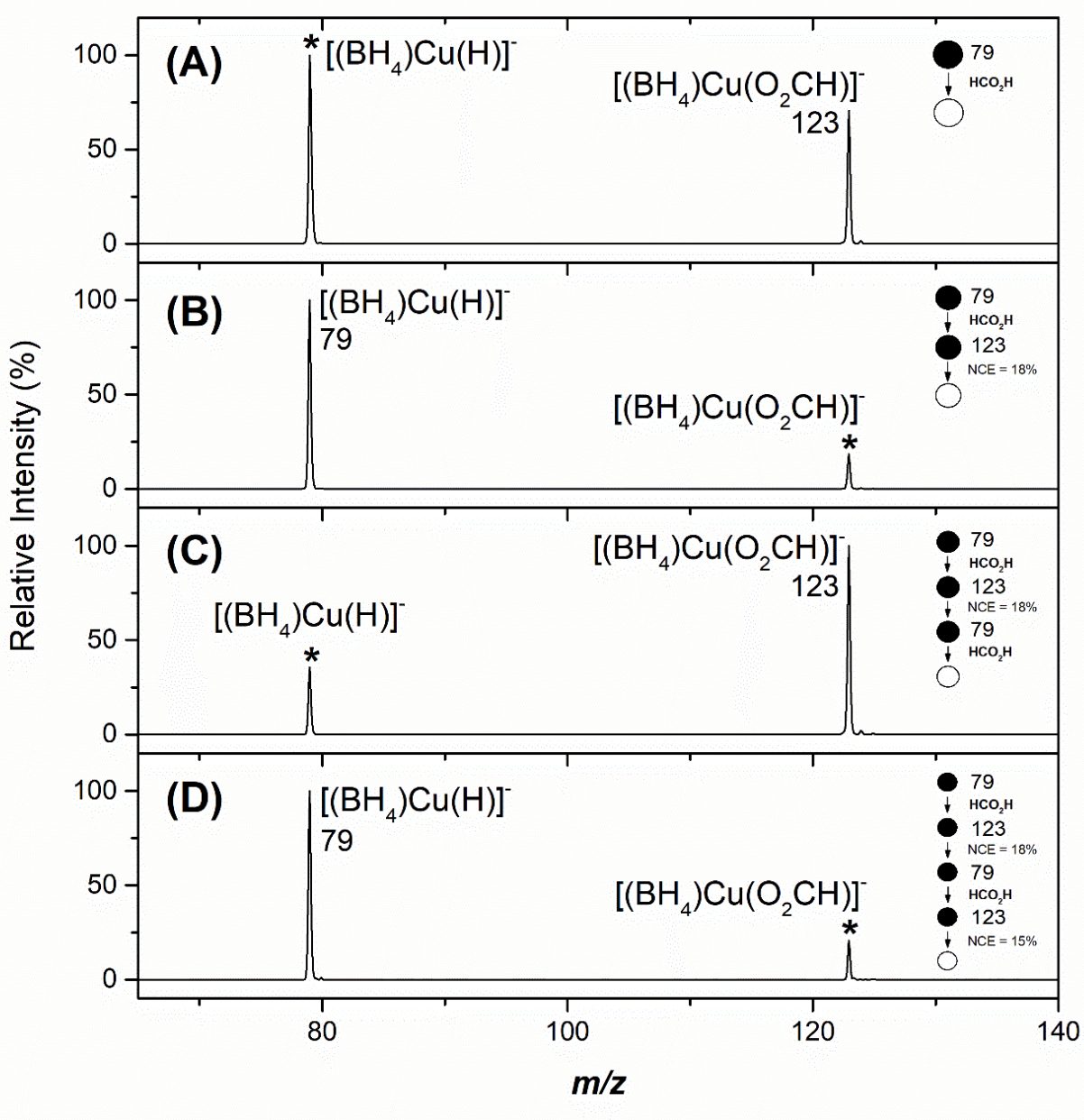

Figure S6. Multistage mass spectrometry (MS^n) on $[(L)Cu(H)]^-$, L = BH_4^-, demonstrating its involvement in a two-step gas-phase catalytic cycle for the selective decomposition of formic acid: (A) MS^2 IMR experiment of $[(BH_4)Cu(H)]^-$ (*m/z* 79), **1_BH4**, with HCO_2H; (B) MS^3 low energy ion trap collision-induced dissociation (CID) experiment on $[(BH_4)Cu(O_2CH)]^-$ (*m/z* 123); (C) MS^4 IMR experiment of $[(BH_4)Cu(H)]^-$ (*m/z* 79), **1_BH4**, with HCO_2H, and; (D) MS^5 low energy ion trap collision-induced dissociation (CID) experiment on $[(BH_4)Cu(O_2CH)]^-$ (*m/z* 123). An asterisk (*) denotes the mass selected precursor ion.

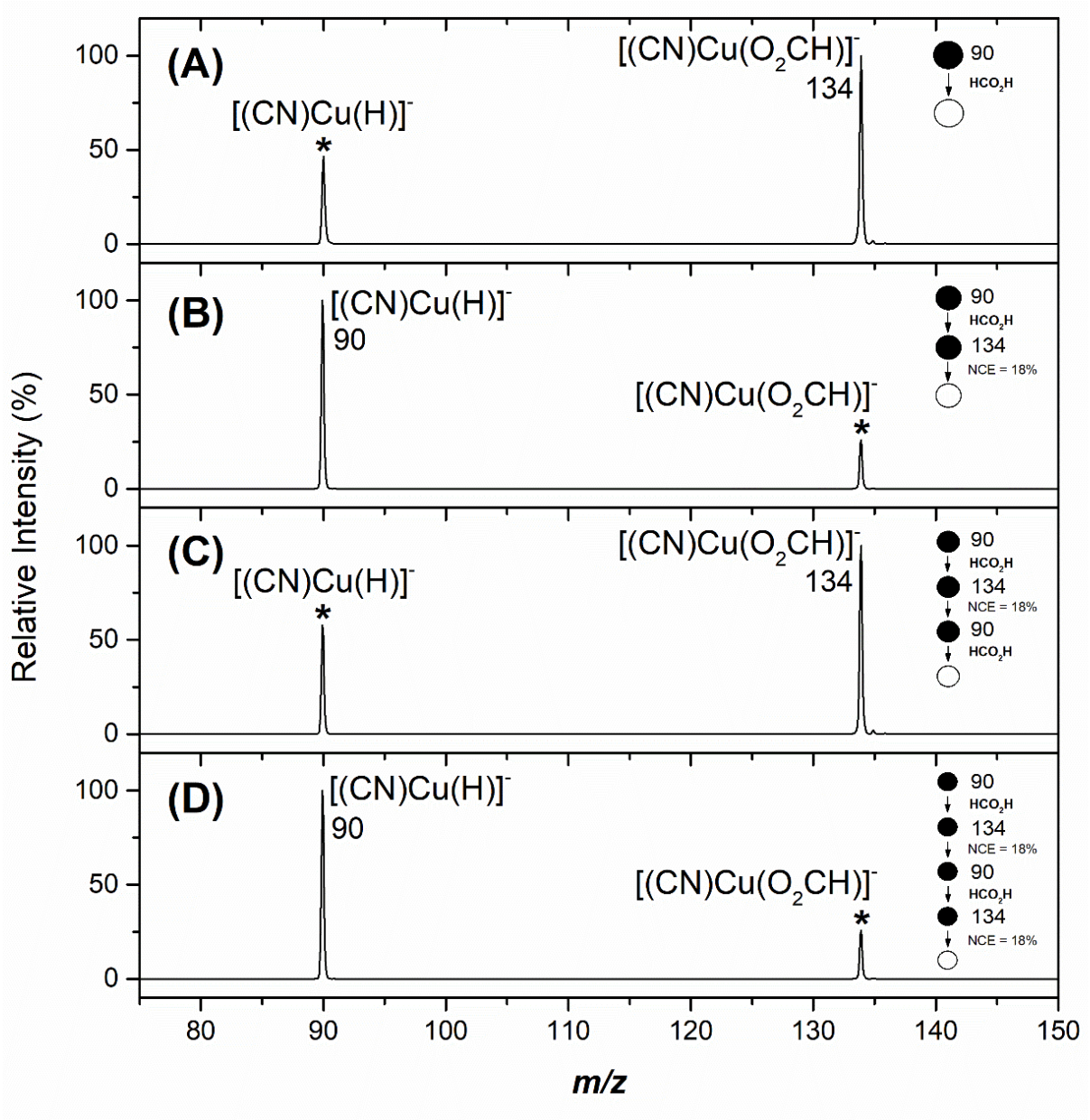

Figure S7. Multistage mass spectrometry (MS^n) on $[(L)Cu(H)]^-$, L = CN^-, demonstrating its involvement in a two-step gas-phase catalytic cycle for the selective decomposition of formic acid: (A) MS^2 IMR experiment of $[(CN)Cu(H)]^-$ (*m/z* 90), **1_CN**, with HCO_2H; (B) MS^3 low energy ion trap collision-induced dissociation (CID) experiment on $[(CN)Cu(O_2CH)]^-$ (*m/z* 134); (C) MS^4 IMR experiment of $[(CN)Cu(H)]^-$ (*m/z* 90), **1_CN**, with HCO_2H, and; (D) MS^5 low energy ion trap collision-induced dissociation (CID) experiment on $[(CN)Cu(O_2CH)]^-$ (*m/z* 134). An asterisk (*) denotes the mass selected precursor ion.

S4. Equations for the IMR between 1_H, 1_O$_2$CH and DCO$_2$H

$$[(H)Cu(H)]^- + DCO_2H \rightarrow [(H)Cu(O_2CD)]^- + H_2 \quad (S1)$$

$$[(H)Cu(O_2CD)]^- \rightarrow [(H)Cu(D)]^- + CO_2 \quad (S2)$$

$$[(H)Cu(D)]^- + DCO_2H \rightarrow [(DCO_2)Cu(D)]^- + H_2 \quad (S3)$$

$[(DCO_2)Cu(D)]^- \rightarrow [(D)Cu(D)]^- + CO_2$ (S4)

$[(D)Cu(D)]^- + DCO_2H \rightarrow [(D)Cu(O_2CD)]^- + HD$ (S5)

$[(H)Cu(O_2CD)]^- + DCO_2H \rightarrow [(DCO_2)Cu(O_2CD)]^- + H_2$ (S6)

$[(DCO_2)Cu(O_2CD)]^- \rightarrow [(DCO_2)Cu(D)]^- + CO_2$ (S7)

$[(DCO_2)Cu(D)]^- + DCO_2H \rightarrow [(DCO_2)Cu(O_2CD)]^- + HD$ (S8)

$[(HCO_2)Cu(H)]^- + DCO_2H \rightarrow [(HCO_2)Cu(O_2CD)]^- + H_2$ (S1a)

$[(HCO_2)Cu(O_2CD)]^- \rightarrow [(H)Cu(O_2CD)]^- + CO_2$ (S2a)

$[(HCO_2)Cu(O_2CD)]^- \rightarrow [(HCO_2)Cu(D)]^- + CO_2$ (S2b)

S5. MS^n IMR spectra with DCO_2H and temporal plots

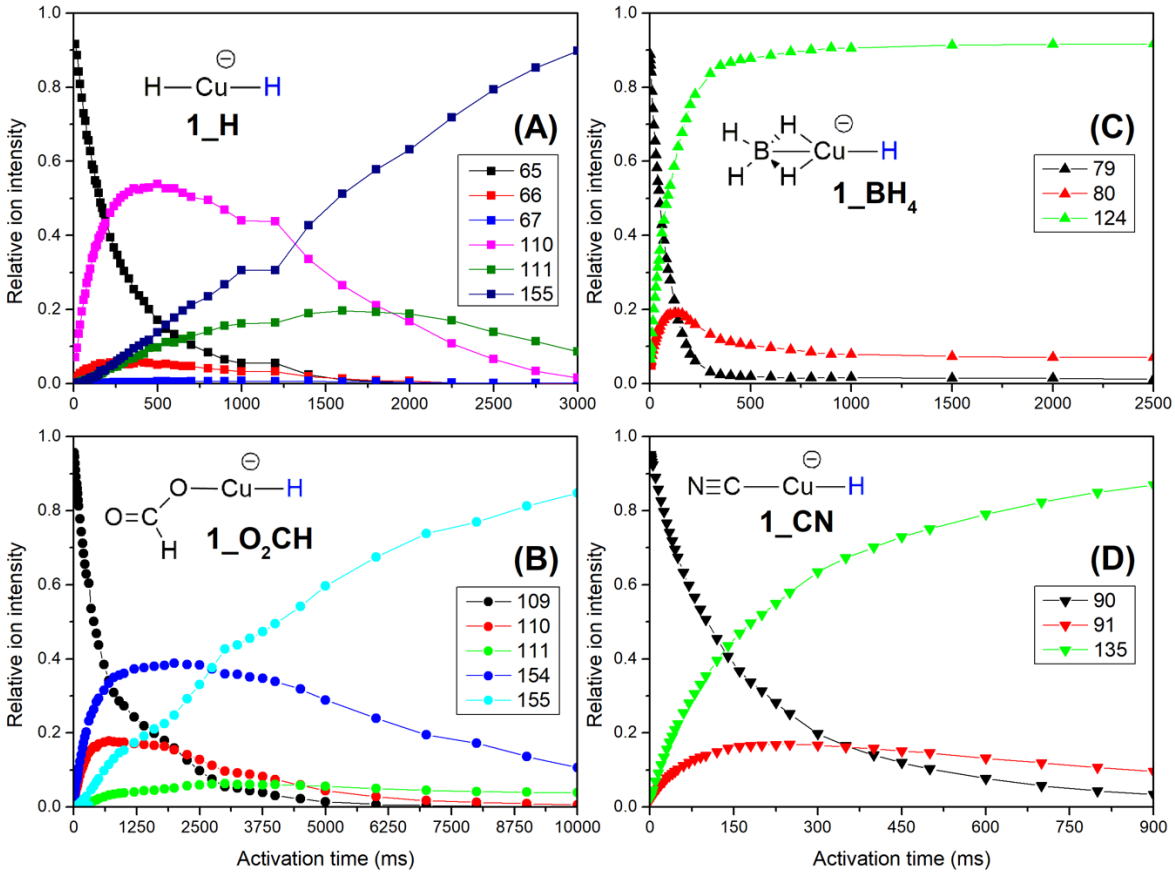

Figure S8. Representative temporal plots for the IMR between $[(L)Cu(H)]^-$ with DCO_2H. Relative ion intensities versus time (ms) for (A) **1_H**, $[(H)Cu(H)]^-$ (*m/z* 65); (B) **1_O₂CH**, $[(HCO_2)Cu(H)]^-$ (*m/z* 109); (C) **1_BH₄**, $[(BH_4)Cu(H)]^-$ (*m/z* 79); (D) **1_CN**, $[(CN)Cu(H)]^-$ (*m/z* 90).

S6. DFT calculated structures and potential energy surfaces

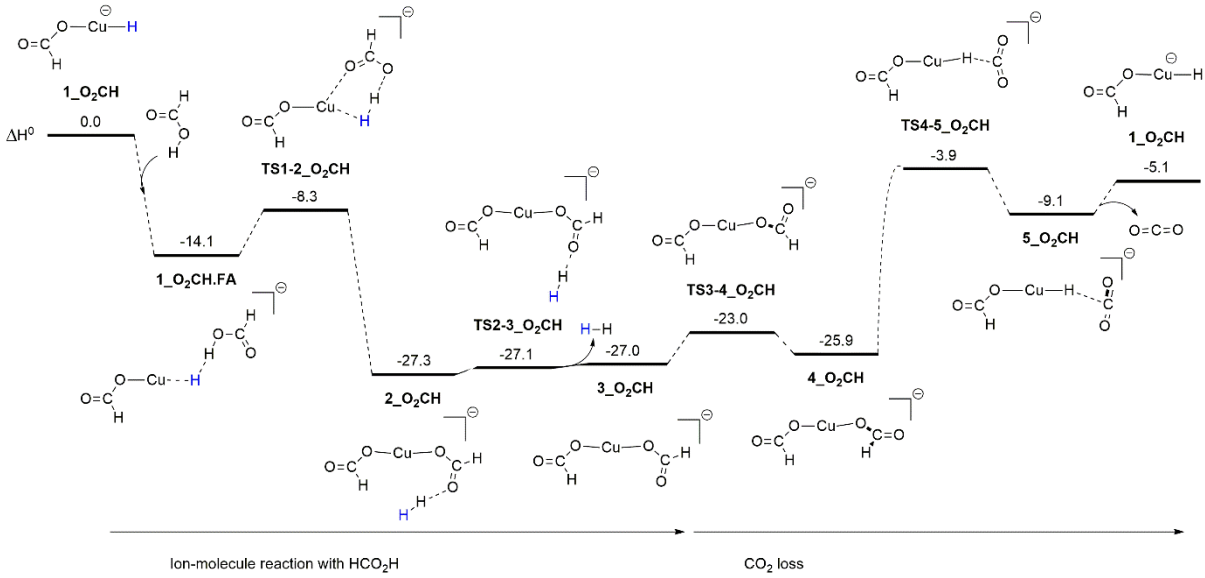

Figure S9. DFT calculated energy surface for the two reaction steps in the catalytic cycle for $[(HCO_2)Cu(H)]^-$. Ion-molecule reaction of $[(HCO_2)Cu(H)]^-$ with HCO_2H followed by subsequent CO_2 loss. The relative enthalpies ΔH^0 (0 K), in parentheses, are given in kcal mol^{-1} and are calculated at the ωB97XD/def2TZVPP level of theory.

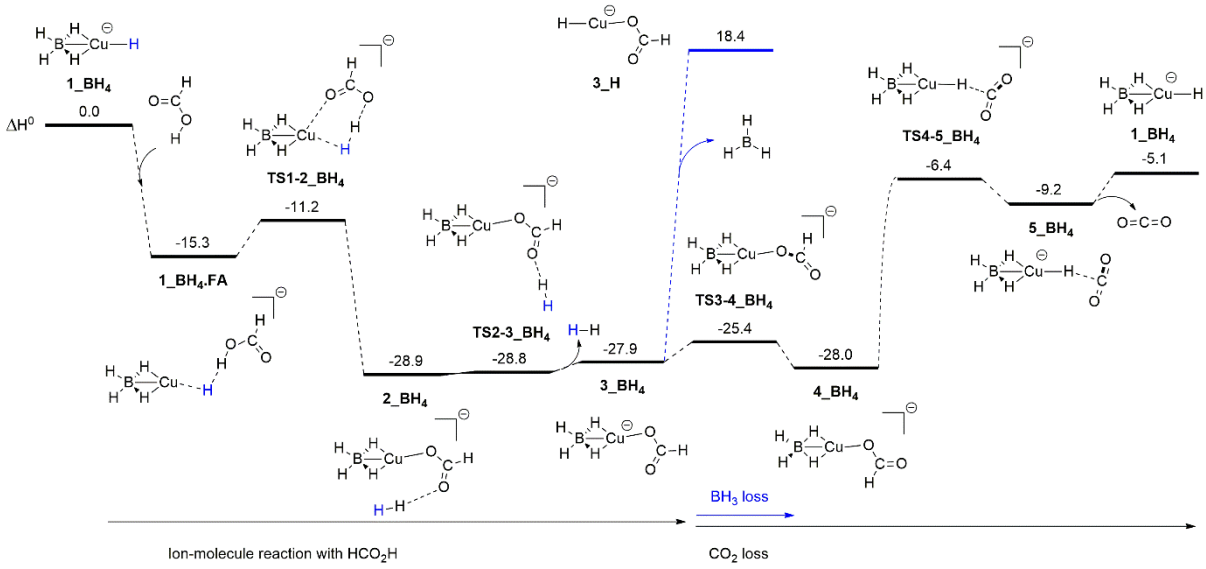

Figure S10. DFT calculated energy surface for the two reaction steps in the catalytic cycle for $[(BH_4)Cu(H)]^-$. Ion-molecule reaction of $[(BH_4)Cu(H)]^-$ with HCO_2H followed by subsequent competing CO_2 or BH_3 (in blue) loss. The relative enthalpies ΔH^0 (0 K), in parentheses, are given in kcal mol^{-1} and are calculated at the ωB97XD/def2TZVPP level of theory.

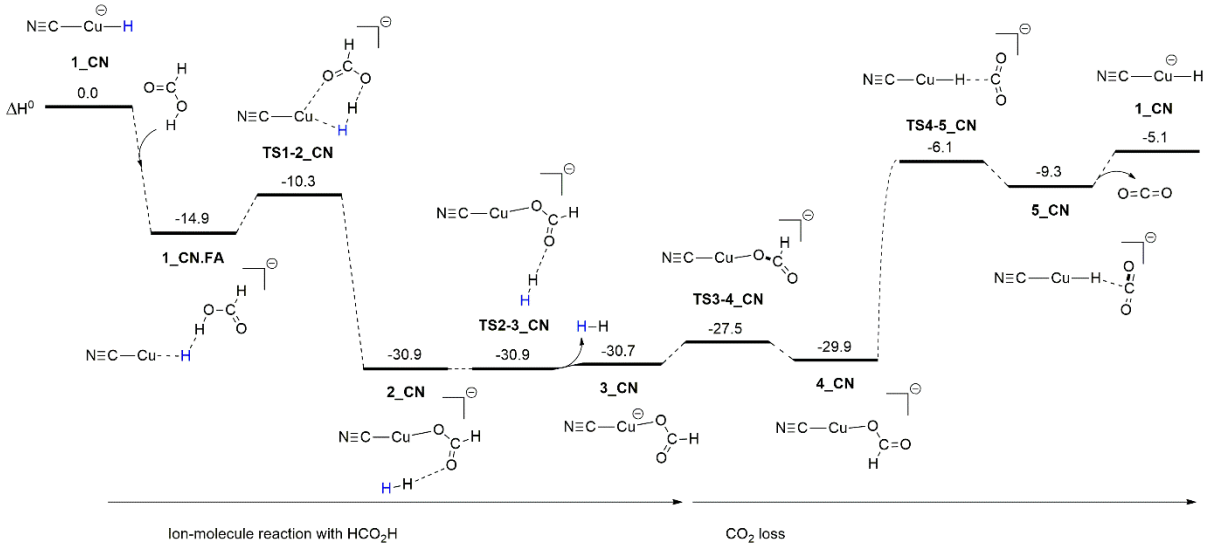

Figure S11. DFT calculated energy surface for the two reaction steps in the catalytic cycle for $[(CN)Cu(H)]^-$. Ion-molecule reaction of $[(CN)Cu(H)]^-$ with HCO_2H followed by subsequent CO_2 loss. The relative enthalpies ΔH^0 (0 K), in parentheses, are given in kcal mol^{-1} and are calculated at the ωB97XD/def2TZVPP level of theory.

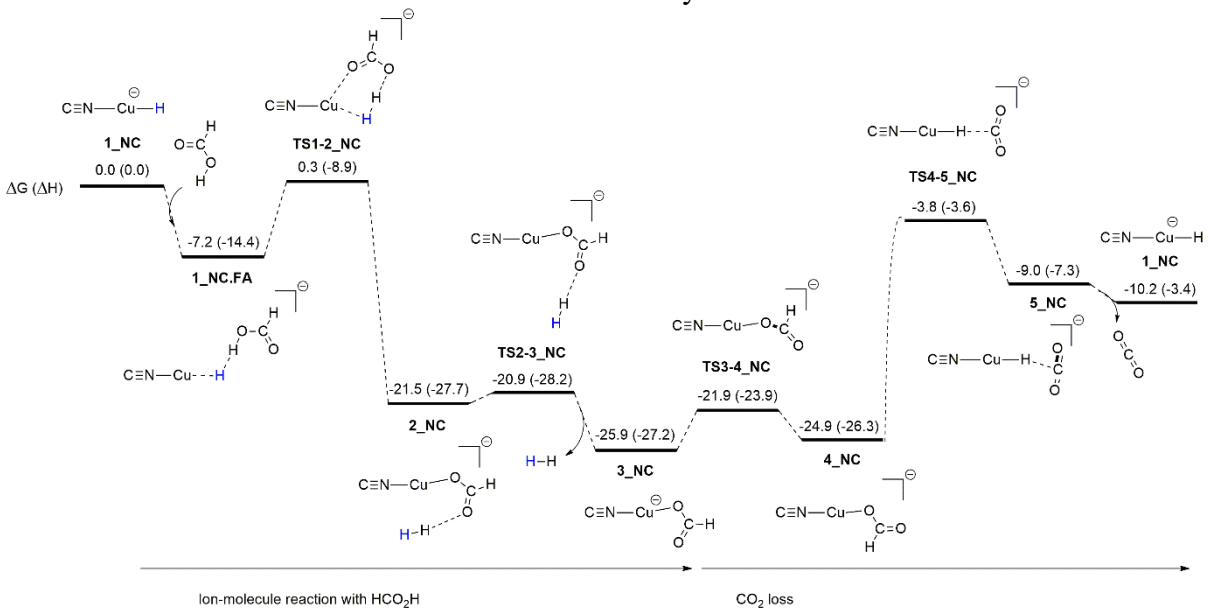

Figure S12. DFT calculated energy surface for the two reaction steps in the catalytic cycle for $[(isoCN)Cu(H)]^-$. Ion-molecule reaction of $[(isoCN)Cu(H)]^-$ with HCO_2H followed by subsequent CO_2 loss. The relative Gibbs free energies ΔG and enthalpies ΔH, in parentheses, are given in kcal mol^{-1} and are calculated at the ωB97XD/def2TZVPP level of theory

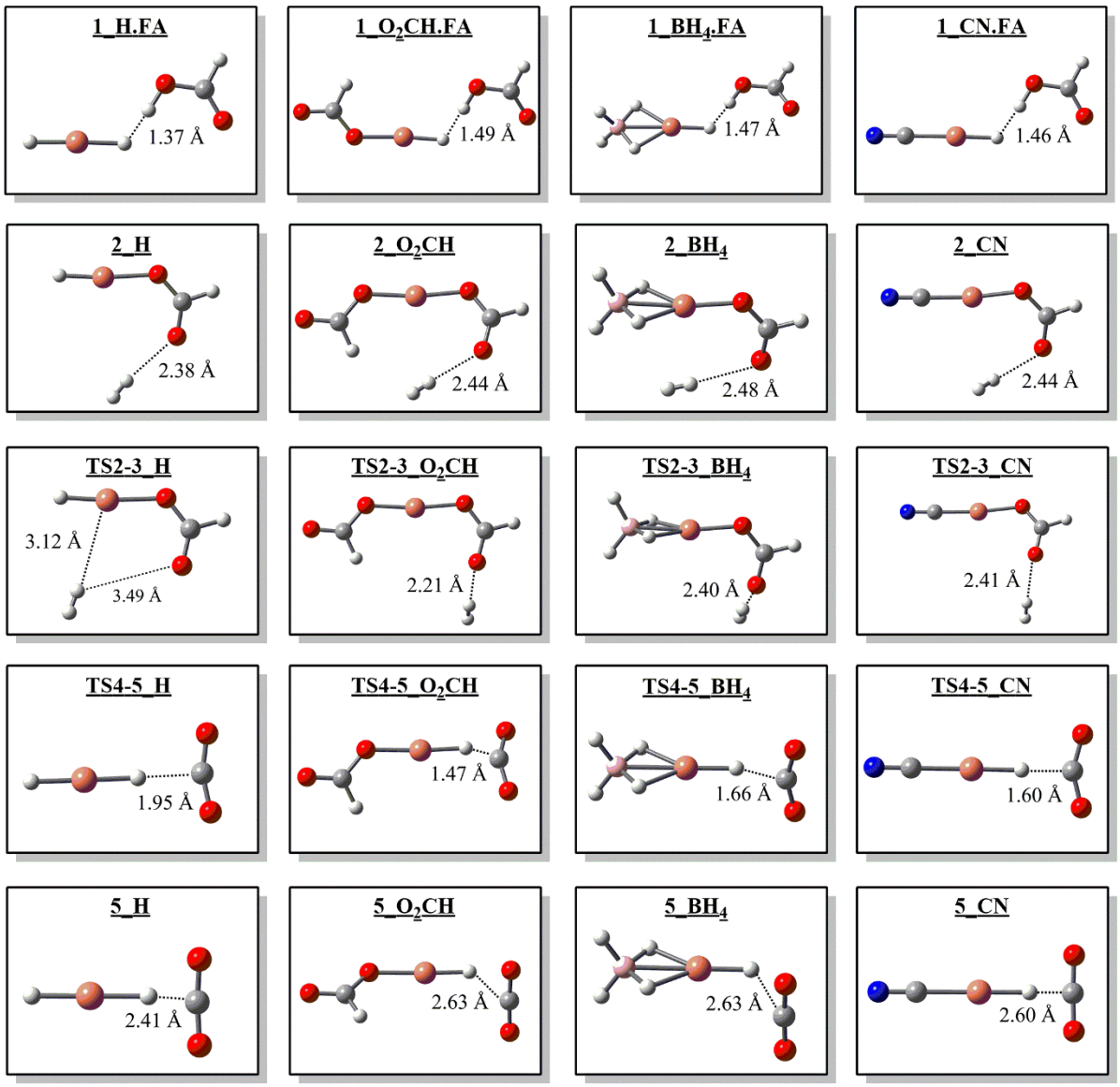

Figure S13. Bond distances of weak interactions in structures **1.FA**, **2**, **TS2-3**, **TS4-5** and **5** for each copper hydride anion species.

S7. Comparison of DFT calculated energies between $[(L)Cu(H)]^-$ with HCO_2H

Table S3. Comparison of DFT calculated energies ΔG (ΔH^0) for the ion-molecule reactions of $[(L)Cu(H)]^-$ (where L = H^-, O_2CH^-, BH_4^-, CN^- and NC^-) with formic acid (HCO_2H), followed by decarboxylation to give $[(L)Cu(H)]^-$, CO_2 and H_2. Energies are given in kcal mol^{-1} and are calculated at the ωB97XD/def2TZVPP level of theory. *ΔH values were used for L = NC^- instead.

	H^-	O_2CH^-	BH_4^-	CN^-	NC^{-*}
1 + HCO_2H	0.0 (0.0)	0.0 (0.0)	0.0 (0.0)	0.0 (0.0)	0.0 (0.0)
1.FA	-12.5 (-19.1)	-5.3 (-14.1)	-8.0 (-15.3)	-7.6 (-14.9)	-7.2 (-14.4)
TS1-2	-7.8 (-15.4)	1.7 (-8.3)	-1.1 (-11.2)	-1.3 (-10.3)	-0.3 (-8.9)
2	-31.9 (-36.8)	-19.2 (-27.3)	-21.4 (-28.9)	-23.6 (-30.9)	-21.5 (-27.7)
TS2-3	-30.4 (-36.6)	-18.5 (-27.1)	-20.3 (-28.8)	-23.0 (-30.9)	-20.9 (-28.2)

3 + H_2	-34.7 (-36.3)	-23.9 (-27.0)	-24.6 (-27.9)	-28.1 (-30.7)	-25.9 (-27.2)
TS3-4 + H_2	-31.9 (-33.9)	-20.8 (-23.0)	-21.7 (-25.4)	-24.5 (-27.5)	-21.9 (-23.9)
4 + H_2	-34.7 (-36.4)	-22.8 (-25.9)	-24.9 (-28.0)	-27.1 (-29.9)	-24.9 (-26.3)
TS4-5 +H_2	-10.9 (-10.7)	-2.0 (-3.9)	-4.7 (-6.4)	-5.8 (-6.1)	-3.8 (-3.6)
5 + H_2	-11.0 (-10.7)	-8.6 (-9.1)	-8.2 (-9.2)	-9.1 (-9.3)	-9.0 (-7.3)
1 + CO_2 + H_2	-10.2 (-5.1)	-10.2 (-5.1)	-10.2 (-5.1)	-10.2 (-5.1)	-10.2 (-3.4)

Table S4. Comparison of DFT calculated energies ΔG (ΔH^0) for the ion-molecule reactions of $[(L)Cu(H)]^-$ (where L = H^-, O_2CH^-, BH_4^-, CN^- and NC^-) with formic acid (HCO_2H), followed by decarboxylation to give $[(L)Cu(H)]^-$, CO_2 and H_2. Energies are given in kcal mol^{-1} and are calculated at the M06-2x-D3/def2TZVP level of theory. $^*\Delta H$ values were used for L = NC^- instead.

	H^-	**O_2CH^-**	**BH_4^-**	**CN^-**	**NC^{-*}**
1 + HCO_2H	0.0 (0.0)	0.0 (0.0)	0.0 (0.0)	0.0 (0.0)	0.0 (0.0)
1.FA	-15.5 (-19.8)	-8.2 (-15.0)	-7.0 (-16.3)	-8.0 (-15.8)	-6.8 (-16.1)
TS1-2	-15.5 (-19.0)	-4.0 (-13.6)	-6.1 (-16.2)	-7.0 (-14.9)	-5.2 (-14.3)
2	-39.7 (-42.2)	-26.3 (-34.8)	-27.6 (-36.2)	-30.4 (-36.9)	-28.2 (-34.8)
TS2-3	-38.9 (-41.9)	-26.7 (-34.6)	-27.8 (-36.1)	-30.3 (-36.9)	-28.3 (-35.2)
3 + H_2	-43.4 (-41.7)	-31.8 (-34.5)	-33.7 (-36.0)	-35.2 (-36.7)	-33.0 (-34.2)
TS3-4 + H_2	-40.4 (-38.9)	-26.9 (-30.1)	-28.7 (-32.1)	-31.2 (-33.0)	-28.8 (-30.6)
4 + H_2	-42.7 (-41.1)	-29.3 (-32.2)	-31.3 (-34.3)	-33.5 (-35.0)	-31.2 (-32.3)
TS4-5 +H_2	-14.4 (-11.2)	-6.1 (-7.6)	-7.9 (-9.1)	-9.0 (-8.5)	-7.4 (-6.8)
5 + H_2	-15.1 (-10.9)	-9.6 (-9.8)	-9.0 (-10.3)	-10.9 (-9.8)	-10.0 (-8.1)
1 + CO_2 + H_2	-10.2 (-5.1)	-10.2 (-5.1)	-10.2 (-5.1)	-10.2 (-5.1)	-10.2 (-3.3)

Table S5. Comparison of DFT calculated energies ΔG (ΔH^0) for the ion-molecule reactions of $[(L)Cu(H)]^-$ (where L = H^-, O_2CH^-, BH_4^-, CN^- and NC^-) with formic acid (HCO_2H), followed by decarboxylation to give $[(L)Cu(H)]^-$, CO_2 and H_2. Energies are given in kcal mol^{-1} and are calculated at the MN15/def2TZVP level of theory. $^*\Delta H$ values were used for L = NC^- instead.

	H^-	**O_2CH^-**	**BH_4^-**	**CN^-**	**NC^-**
1 + HCO_2H	0.0 (0.0)	0.0 (0.0)	0.0 (0.0)	0.0 (0.0)	0.0 (0.0)
1.FA	-12.5 (-19.3)	-6.9 (-14.2)	-7.7 (-15.2)	-8.6 (-14.5)	-7.5 (-14.5)
TS1-2	-9.2 (-17.2)	-1.5 (-11.3)	-3.5 (-13.9)	-4.6 (-12.5)	-2.5 (-11.6)
2	-32.9 (-39.2)	-22.3 (-30.5)	-23.6 (-31.8)	-26.8 (-33.1)	-24.3 (-30.5)
TS2-3	-31.9 (-38.8)	-21.5 (-29.7)	-23.1 (-31.3)	-26.5 (-32.8)	-23.8 (-30.6)
3 + H_2	-36.3 (-38.3)	-26.2 (-29.4)	-27.7 (-30.9)	-30.9 (-32.4)	-28.2 (-29.5)
TS3-4 + H_2	-33.4 (-35.7)	-21.9 (-25.2)	-23.9 (-27.4)	-27.3 (-29.1)	-24.2 (-26.0)
4 + H_2	-36.1 (-38.2)	-24.8 (-27.9)	-26.6 (-30.0)	-29.9 (-31.4)	-27.0 (-28.2)
TS4-5 +H_2	-11.4 (-11.9)	-4.2 (-5.6)	-5.6 (-7.5)	-6.8 (-6.8)	-5.0 (-4.8)
5 + H_2	-11.5 (-11.9)	-9.5 (-10.1)	-9.2 (-10.4)	-10.8 (-9.7)	-10.0 (-8.2)
1 + CO_2 + H_2	-10.3 (-5.2)	-10.3 (-5.2)	-10.3 (-5.2)	-10.3 (-5.2)	-10.3 (-3.5)

Table S6. Comparison of DFT calculated energies ΔG (ΔH^0) for the ion-molecule reactions of $[(L)Cu(H)]^-$ (where L = H^-, O_2CH^-, BH_4^-, CN^- and NC^-) with formic acid (HCO_2H), followed by decarboxylation to give $[(L)Cu(H)]^-$, CO_2 and H_2. Energies are given in kcal mol^{-1} and are

calculated at the CAM-B3LYP-D3BJ/def2TZVP level of theory. *ΔH values were used for L = NC^- instead.

	H^-	**O_2CH^-**	**BH_4^-**	**CN^-**	**NC^-**
1 + HCO_2H	0.0 (0.0)	0.0 (0.0)	0.0 (0.0)	0.0 (0.0)	0.0 (0.0)
1.FA	-14.3 (-21.0)	-7.9 (-15.3)	-8.9 (-16.5)	-10.5 (-15.8)	-10.1 (-15.2)
TS1-2	-10.4 (-17.9)	-1.1 (-10.8)	-3.4 (-13.6)	-5.4 (-12.4)	-3.8 (-11.1)
2	-34.0 (-39.9)	-22.6 (-30.2)	-24.1 (-31.9)	-29.1 (-33.3)	-26.7 (-30.2)
TS2-3	-33.2 (-39.4)	-22.0 (-30.2)	n/a†	-27.8 (-33.4)	-25.5 (-30.8)
3 + H_2	-37.5 (-39.2)	-26.7 (-29.7)	-28.4 (-31.3)	-32.2 (-32.9)	-30.0 (-29.5)
TS3-4 + H_2	-34.8 (-36.7)	-22.4 (-25.7)	-24.4 (-28.0)	-28.7 (-29.7)	-26.1 (-26.2)
4 + H_2	-37.5 (-39.2)	-25.4 (-28.5)	-27.3 (-30.6)	-31.3 (-32.1)	-29.0 (-28.4)
TS4-5 +H_2	n/a‡	-3.1 (-5.1)	-6.0 (-7.5)	-8.3 (-6.7)	-6.0 (-4.2)
5 + H_2	n/a‡	-9.0 (-9.1)	-8.8 (-9.4)	-11.0 (-8.9)	-10.6 (-6.9)
1 + CO_2 + H_2	-9.6 (-4.5)	-9.6 (-4.5)	-9.6 (-4.5)	-9.6 (-4.5)	-9.6 (-2.8)

† TS2-3_BH_4 could not be located at the CAM-B3LYP-D3BJ/def2TZVP level of theory. IRC calculations on TS1-2_BH_4 suggest that upon forming the coordinated formate, the H_2 immediately dissociates from the $[(BH_4)Cu(O_2CH)]^-$ ion without requiring TS2-3_BH_4. ‡ TS4-5_H and 5_H could not be located at the CAM-B3LYP-D3BJ/def2TZVP level of theory.

S8. Comparison of energetics for BH_3 vs. CO_2 loss in the PES between 1_BH_4 and HCO_2H

Table S7. DFT calculated energetics (ΔH^0, ΔH and ΔG) for BH_3 loss vs. CO_2 loss from **3_BH_4** $[(BH_4)Cu(O_2CH)]^-$ at different levels of theory. Energies are given in kcal mol^{-1}.

	ΔH^0		**ΔH**		**ΔG**	
	BH_3 loss	CO_2 loss	BH_3 loss	CO_2 loss	BH_3 loss	CO_2 loss
ωB97XD	46.3	22.8	47.0	23.0	37.3	14.4
M06-2X-D3	49.7	30.9	50.3	31.0	41.8	33.5
MN15	53.5	25.7	54.1	25.9	44.7	17.5
CAM-B3LYP-D3BJ	47.0	26.8	47.6	26.9	38.4	18.8